DC–110-GHz MMIC Traveling-Wave Switch

Hiroshi Mizutani, *Member, IEEE,* and Yoichiro Takayama, *Member, IEEE*

***Abstract*—This paper presents the broadest band monolithic-microwave integrated-circuit traveling-wave switch ever reported for millimeter-wave applications. The developed switch with the novel structure of a 400-μm-gate finger field-effect transistor (FET) indicated an insertion loss of less than 2.55 dB and an isolation of better than 22.2 dB from dc to 110 GHz. Also, the switch indicated no degradation of an insertion loss and an ON/OFF ratio of more than 22.7 dB up to an input power of 26.5 dBm at 40 GHz. Circuit analytical results based on a lossy transmission-line model for small-signal performance and circuit simulation results using the two-terminal nonlinear FET model for large-signal operation successfully showed good agreement with the experimental results.**

***Index Terms*—Distributed FET, millimeter-wave, MMIC switch, modeling, nonlinear circuit, traveling wave.**

I. Introduction

FOR communication and radar systems, transmitter/receiver (T/R) switches play an important role to control the RF signal flow. In these applications, a broad-band switch with high power-handling capability and high switching speed is strongly required for low-cost system realization.

Recently, several FET switch circuits have been reported for the millimeter-wave applications [1]–[6]. Especially beyond 60 GHz, four types of FET switch circuit configuration providing a high isolation of over 20 dB have been reported [2]–[6]. The first type has the shunt configuration in conjunction with a quarter-wavelength transformer for single-pole double-throw (SPDT) switches, which have a high isolation of 25 dB and an insertion loss of 1.5 dB from 59 to 61 GHz [2]. The second type of switch circuit has the series FET configuration with a parallel inductor, and the switch has shown an insertion loss of 1.6 dB and an isolation of over 20 dB at 94 GHz [3]. This type of switch forms a resonant circuit with the capacitor in the pinched-off state of the FET and the inductor externally connected between the source and drain. However, the resonant frequency of this switch circuit is sensitive to variations of the pinched-off-state capacitance. The third type has a circuit using the parallel resonance between a capacitive stub and an inductive shunt line, and it showed an insertion loss of 3.9 dB and an isolation of 41 dB at 60 GHz [4]. These configurations are restricted to narrow-band applications. The last type has a circuit with the series-shunt configuration incorporating the ohmic electrode sharing technology (OEST) to diminish the parasitic capacitance for broad-band characteristics [5]. This monolithic-microwave integrated-circuit (MMIC) switch showed high performance with insertion loss of less than 1.64 dB and isolation of better than 20.6 dB from dc to 60 GHz. From the viewpoint of the broad-band characteristics, the so-called distributed switch circuits have been reported, which are treated as an artificial transmission line, which consists of the finite combination of a unit series inductor and a unit shunt discrete FET used as a pinched-off-state capacitor [6]. The broad-band MMIC switch having a novel distributed FET structure, which provides excellent performance from dc to 60 GHz, was reported [9]. The small-signal characteristics of this switch were expressed by the lossless transmission-line model for the ON state and the lossy transmission line model for the OFF state.

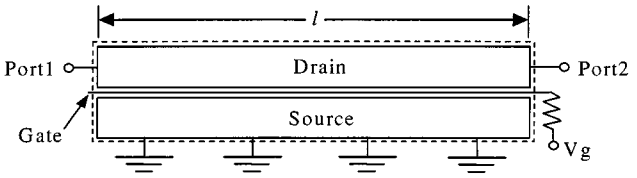

Fig. 1. Schematic view of the TWSW (source electrode is grounded by four via-holes).

In this paper, the state-of-the-art broad-band characteristics of the MMIC traveling-wave switch (TWSW) will be newly evaluated from dc to 110 GHz. A more precise analytical model with the lossy transmission-line model for both ON and OFF states will be presented, which fully accounts for measured small-signal characteristics. The power transfer capability and the switching speed of the developed MMIC switch have been also evaluated. The large-signal operation of the TWSW will be discussed by introducing the two-terminal nonlinear FET model [5] for both the ON and OFF states, which indicates good agreement with the measured data.

II. Circuit Design

The novel MMIC TWSW has been developed. The TWSW is schematically shown in Fig. 1, and the corresponding equivalent-circuit diagram is shown in Fig. 2. An RF signal is impressed on port 1 at one end of the drain electrode, and the output signal appears at port 2 on the other end of the drain electrode if the switch is in the ON state. A control voltage V_g is applied to the gate through an isolation resistor of the order of 10 kΩ. The TWSW is expressed as the combination of a distributed shunt FET and a transmission line of drain electrode. Since the gate bias circuit is isolated with a sufficiently large value resistor, the distributed FET in the open-channel state is expressed as a simple distributed resistor, and in the pinched-off state, approximately a simple distributed capacitor.

For both the ON and OFF states of the TWSW, the equivalent circuit is expressed as shown in Fig. 3. This is the same circuit

Manuscript received April 6, 1999.

H. Mizutani is with the C&C LSI Development Division, NEC Corporation, Kawasaki 211-8666, Japan (e-mail: mizutani@lsi.nec.co.jp).

Y. Takayama is with the Semiconductor Group, NEC Corporation, Kawasaki 211-8666, Japan.

Publisher Item Identifier S 0018-9480(00)03763-7.

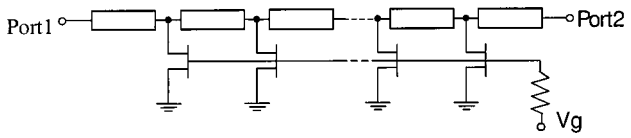

Fig. 2. Equivalent circuit of TWSW.

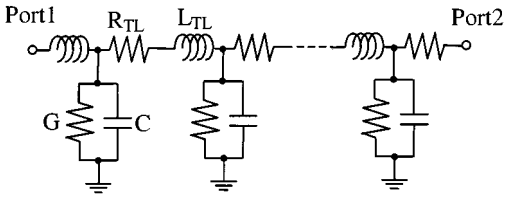

Fig. 3. Equivalent circuit of the TWSW with lossy transmission-line model $G = 0, C = C_{\rm TL} + C_{\rm FET}$ for the ON state $G = G_{\rm FET}, C = C_{\rm TL}$ for the OFF state.

as a lossy transmission line. Thus, the insertion loss and the isolation of the TWSW can be expressed as the same formula, derived as

$$S_{21} = \frac{2ZZ_0}{2ZZ_0 \cosh \gamma\ell + (Z^2 + Z_0^2) \sinh \gamma\ell}. \tag{1}$$

The return loss is also derived as

$$S_{11} = \frac{(Z^2 - Z_0^2) \sinh \gamma\ell}{2ZZ_0 \cosh \gamma\ell + (Z^2 + Z_0^2) \sinh \gamma\ell} \tag{2}$$

where Z_0 is the port impedance (usually 50 Ω). Z, ℓ, and γ are the characteristic impedance, the physical length of the drain electrode, and the propagation constant, respectively. For the ON state, γ and Z are expressed as

$$\begin{aligned}\gamma &\equiv \alpha + j\beta \\ &\equiv \sqrt{j\omega(R_{\rm TL} + j\omega L_{\rm TL})(C_{\rm TL} + C_{\rm FET})}\end{aligned} \tag{3}$$

$$Z = \sqrt{\frac{R_{\rm TL} + j\omega L_{\rm TL}}{j\omega(C_{\rm TL} + C_{\rm FET})}} \tag{4}$$

and for the OFF state

$$\begin{aligned}\gamma &\equiv \alpha + j\beta \\ &\equiv \sqrt{(R_{\rm TL} + j\omega L_{\rm TL})(G_{\rm FET} + j\omega C_{\rm TL})}\end{aligned} \tag{5}$$

$$Z = \sqrt{\frac{R_{\rm TL} + j\omega L_{\rm TL}}{G_{\rm FET} + j\omega C_{\rm TL}}} \tag{6}$$

where $R_{\rm TL}$, $L_{\rm TL}$, and $C_{\rm TL}$ are the series resistance, inductance, and capacitance per unit length of the drain electrode transmission line, respectively. $C_{\rm FET}$ is the capacitance of the unit FET in the pinched-off state. $G_{\rm FET}(=1/R_{\rm FET})$ is the conductance for the unit FET in the open-channel state, which corresponds to the shunt conductance per unit length of the lossy transmission line. ω is the angular frequency. The series resistance $R_{\rm TL}$ is proportional to the square root of the frequency because of the skin effect, and can be expressed as

$$R_{\rm TL} = \chi\sqrt{f} \tag{7}$$

where χ is the proportional factor.

TABLE I
PARAMETER VALUE FOR 100-μm-LENGTH FET $R_{\rm FET}$ FOR OPEN-CHANNEL STATE AND $C_{\rm FET}$ FOR PINCHED-OFF STATE

$R_{FET}(=1/G_{FET})$	8.6 Ω
C_{FET}	20 fF
χ	$3.15\text{X}10^{-6}$ Ω/Hz$^{1/2}$
L_{TL}	40 pH
C_{TL}	7 fF

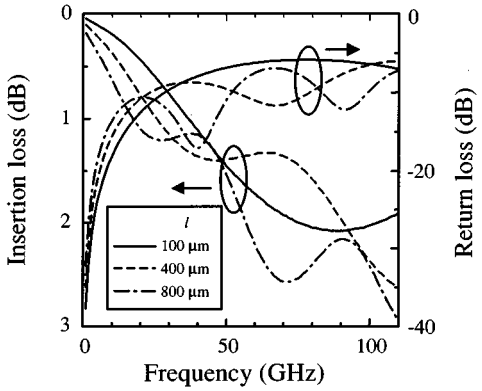

Fig. 4. Calculated insertion loss for 100-, 400-, and 800-μm TWSW's.

The switch was designed with 0.15-μm gate-length heterojunction field-effect transistor (HJFET) technology. From our several examinations, the design parameters for the switch have been extracted. The parameter values for the 100-μm-length FET and a drain–electrode transmission line with the 10-μm width are listed in Table I. From (1) to (4), ideally if $R_{\rm TL} = 0$, the TWSW is equivalent to the lossless transmission line [9]. In this case, the insertion loss of the TWSW is only due to the impedance mismatching between the port and switch, and the insertion loss oscillates periodically with the frequency. If Z is equal to Z_0, the insertion loss is zero and the return loss is infinity. From these equations, it can be expected that the TWSW will show no frequency limit as long as the transmission loss would be negligible. Since actual $R_{\rm TL}$ of the TWSW is not too small to neglect, the insertion loss monotonically increases with the frequency. As seen later, this lossy transmission-line model explains the measured results very well in spite of their simplicity.

Fig. 4 shows the calculated insertion losses and the return losses for the ON state 100-, 400-, and 800-μm TWSW's using (1)–(4) and (7). The insertion loss tends to increase with respect to frequency for each length of the TWSW. The difference between the insertion losses of each length of the TWSW is almost within 0.6 dB from dc to 110 GHz. The return loss ripples with

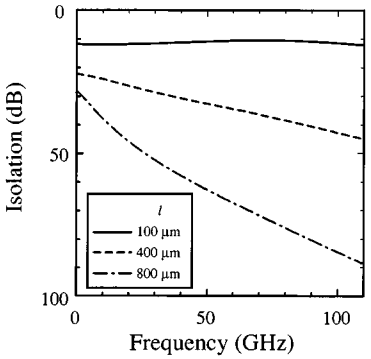

Fig. 5. Calculated isolation for 100-, 400-, and 800-μm TWSW's.

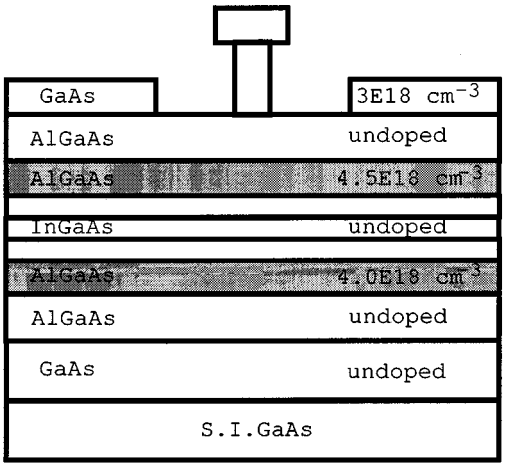

Fig. 6. Cross-sectional view of HJFET.

respect to frequency due to the input impedance mismatching. The calculated isolations for 100-, 400-, and 800-μm TWSW's using (1) and (5)–(7) are shown in Fig. 5. The isolation of the 100-μm TWSW is almost constant with respect to frequency because the 100-μm-finger FET seems to be a lumped element. The calculated isolation of the more than 100-μm TWSW shows the monotonic increase with respect to frequency. The gradient of the isolation to the frequency increases with the increase of TWSW length. The main design scheme of the TWSW is the determination of the physical drain electrode length of the TWSW so as to meet the demanded specification of the insertion loss and isolation. From the return loss in Fig. 4, the impedance mismatching obviously causes over 0.45-dB insertion loss. To realize better input-impedance matching for the ON state, the drain electrode width, which determines $L_{\rm TL}$ and $C_{\rm TL}$, must be chosen optimally.

III. MMIC Design and Fabrication

The TWSW was fabricated using the 0.15-μm HJFET MMIC process for millimeter-wave applications with high reliability [7], [8]. Fig. 6 shows a cross-sectional view of the HJFET. The FET channel structure was optimized so that the MMIC switch can exhibit high current handling capability, as well as high breakdown voltages. A double heterojunction structure was employed. N-type AlGaAs carrier supply layers are placed both

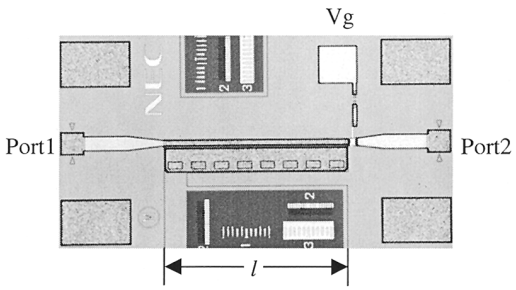

Fig. 7. Top view of developed 400-μm TWSW.

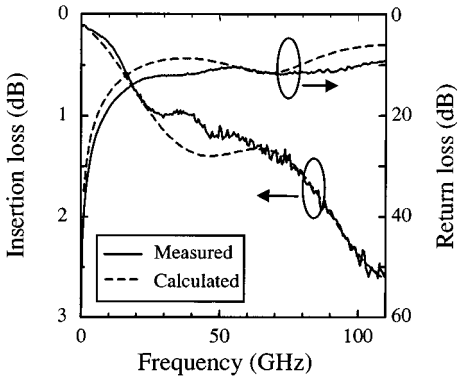

Fig. 8. Measured and calculated insertion and return losses of the ON-state TWSW ($V_g = -5$ V).

above and below the undoped InGaAs channel layer. Typical FET characteristics were as follows. The maximum drain current was 600 mA/mm with a threshold voltage of -2 V, and a reverse gate breakdown voltage of over 10 V. f_T and $f_{\rm max}$ were more than 50 and 180 GHz, respectively. The isolation resistor was monolithically fabricated using the same epitaxial layers used for the FET. To reduce the size of the isolation resistor, the GaAs contact layer between ohmic contacts was removed by selective wet etching. The value of the isolation resistor was of the order of 10 kΩ. A top view of the developed TWSW MMIC is shown in Fig. 7 for a 400-μm-gate finger FET with a 10-μm-width drain electrode. The TWSW consists of a single 0.15-μm-gate FET with the gate finger of 400 μm, which operates as the TWSW. The RF signal input and output terminals are attached on both ends of the drain electrode, respectively. The TWSW is obviously different from the previous distributed switches because of introducing the distributed FET. The size of the TWSW is 0.4 mm $\times$ 0.07 mm for s 400-μm-gate finger FET. The total chip size is 0.85 mm $\times$ 0.45 mm.

IV. MMIC Performance

RF performances for the fabricated MMIC switch were measured from dc to 110 GHz by using an on-wafer probing system with an automatic vector network analyzer (HP85109C). Fig. 8 shows the measured insertion loss and the ON-state return loss for the developed MMIC switch using the 400-μm distributed FET with the calculated results. The distributed FET was controlled with the gate bias voltage V_g. For the ON-state measurement, V_g was set to -5 V. The measured insertion loss was unchanged for V_g less than the FET pinch-off voltage of -2.35 V.

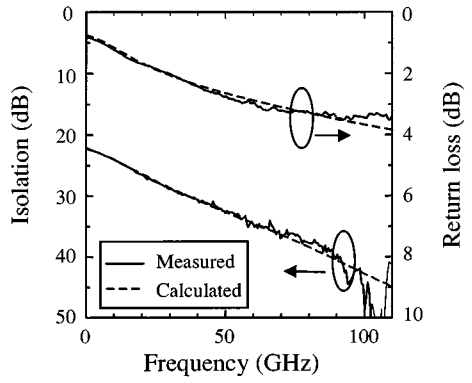

Fig. 9. Measured and calculated isolation and return loss of the OFF-state TWSW ($V_g = 0$ V).

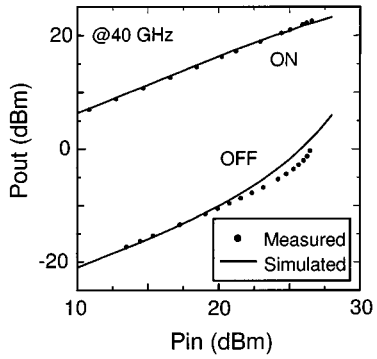

Fig. 10. Measured and simulated power transfer curves ($V_g = -5$ V for ON state and $V_g = 0$ V for OFF state).

In contrast, for the OFF state, V_g was set to 0 V. The measured curves are in excellent agreement with the calculated results on the lossy transmission-line model. At 76, 94, and 110 GHz, the measured insertion losses were 1.52, 2.13, and 2.55 dB, respectively. From dc to 100 GHz, the measured return loss for the ON state was better than 10 dB. To reduce the insertion and return losses, it is important to eliminate the impedance mismatching and the resistance $R_{\rm TL}$, as mentioned above. The 10-dB return loss implies 0.45-dB insertion loss. An improvement of the return loss is expected from reducing the linewidth of the drain electrode. Fig. 9 shows the measured isolation and the return loss for the OFF state of the developed MMIC switch for the 400-μm TWSW. The measured curves indicated excellent agreement with the calculated ones. The measured isolations were better than 22.2 dB with the monotonic increase of over 40 dB from dc to 110 GHz. (i.e., at 76 GHz, the measured isolation was 36.6 dB.)

The power-handling capability was measured at 40 GHz. Fig. 10 shows the measured results up to the input power of 26.5 dBm for both the ON and OFF states. The insertion loss was almost constant through the measured input level. The isolation was gradually degraded over around a 20-dBm input level. The ON/OFF ratio was kept to be over 22.7 dB through the measured input level. The measured insertion loss for the power-handling capability slightly increased compared with the small-signal insertion loss because the wires bonded to the input terminal of the MMIC chip cause further input impedance mismatching.

The switching speed of the developed MMIC has been measured at 20 GHz, applying 50 MHz, 50% duty pulse signal to the gate of the distributed FET. The output signal and input control pulse are shown in Fig. 11. The rise/fall time of the input pulse were 34/32 ps, and the measured rise and fall time of the TWSW for the RF signal were less than 600 and 400 ps, respectively.

V. Discussion

In this section, the large-signal operation will be discussed. The equivalent circuit of the TWSW for the large-signal operation is shown in Fig. 12. The two-terminal nonlinear FET model has been introduced, which consists of the constant capacitor and current source [5]. The length of the 400-μm TWSW was divided into 40 unit FET's with the length of 10 μm. The measured *I–V* characteristics of the unit current source for the open-channel state and the pinched-off state are shown in Fig. 13 by the dots. By using the two-terminal nonlinear FET model, these *I–V* characteristics for the open-channel state are expressed as

$$I\,\mathrm{ds}_O = \begin{cases} \beta(-R_{\rm Iso}Ig_O + \phi_B - V_T)^2 \tanh(\alpha V_{\rm ds}), \\ \quad V_{\rm ds} \le -\phi_B \end{cases} \tag{8}$$

$$\begin{cases} \beta\left(V_{\mathrm{gs}_O} - V_{\rm ds} - V_T\right)^2 \tanh\left(\alpha V_{\rm ds}\right), \\ \quad -\phi_B \le V_{\rm ds} \le 0 \end{cases} \tag{9}$$

$$\beta\left(V_{\mathrm{gs}_O} - V_T\right)^2 \tanh\left(\gamma V_{\rm ds}\right), \qquad 0 \le V_{\rm ds} \tag{10}$$

and

$$Ig_O = \begin{cases} 0, & -\phi_B \le V_{\rm ds} \end{cases} \tag{11}$$

$$\begin{cases} Is_G\Big\{\exp\left[\kappa_f\left(V_{\mathrm{gs}_O} - V_{\rm ds} - \phi_B\right)\right] - 1\Big\}, \\ \quad V_{\rm ds} \le -\phi_B \end{cases} \tag{12}$$

For the pinched-off state, the current source are expressed as

$$I_{\mathrm{ds}_P} = \begin{cases} \beta(-R_{\rm Iso}Ig_P + \phi_B - V_T)^2 \tanh(\alpha V_{\rm ds}), \\ \quad V_{\rm ds} \le V_{\mathrm{gs}_P} - \phi_B \end{cases} \tag{13}$$

$$\beta\left(V_{\mathrm{gs}_P} - V_{\rm ds} - V_T\right)^2 \tanh(\alpha V_{\rm ds}), \tag{14}$$

$$V_{\mathrm{gs}_P} - \phi_B \le V_{\rm ds} \le V_{\mathrm{gs}_P} - V_T \tag{15}$$

$$\begin{cases} 0, & V_{\mathrm{gs}_P} - V_T \le V_{\rm ds} \le V_B \\ Is_D\Big\{\exp\left[\kappa_r\left(V_{\rm ds} - V_B\right)\right] - 1\Big\}, & V_B \le V_{\rm ds} \end{cases} \tag{16}$$

and

$$Ig_P = \begin{cases} 0, & V_{\mathrm{gs}_P} - \phi_B \le V_{\rm ds} \end{cases} \tag{17}$$

$$\begin{cases} Is_G\Big\{\exp[\kappa_f(V_{\mathrm{gs}_P} - V_{\rm ds} - \phi_B)] - 1\Big\}, \\ \quad V_{\rm ds} \le V_{\mathrm{gs}_P} - \phi_B \end{cases} \tag{18}$$

where β is the transconductance parameter, ϕ_B is the build-in potential, V_T is the threshold voltage, Is_G is the gate forward current parameter, I_{s_D} is the drain breakdown current parameter, I_{g_O} is the forward-biased gate current, and I_{g_P} is the reverse-gate breakdown current. V_{gs_O} and V_{gs_P} are the gate–source voltages for the open-channel state and for the pinched-off state, respectively, and V_B is the drain breakdown voltage in the pinched-off state. α, γ, κ_f, and κ_r are the voltage scaling factors. The calculated curves were evaluated by using the FET model parameter shown in Table II. $C_{\rm FET}$ was extracted to be 20 fF. The calculated *I–V* curves indicate good agreement with the measured ones, as shown in Fig. 13.

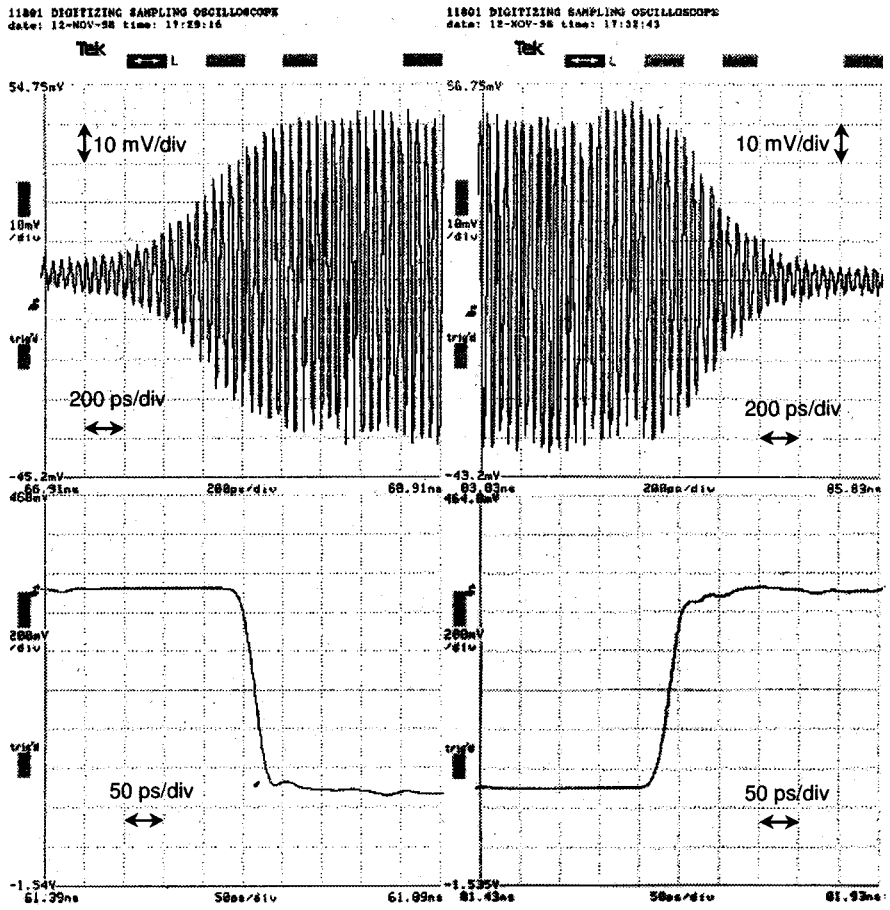

Fig. 11. Measured switching speed at 20 GHz with 50 MHz, 50% duty applied pulse.

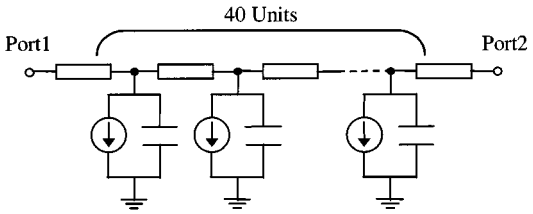

Fig. 12. Equivalent circuit of TWSW using two-terminal nonlinear FET model.

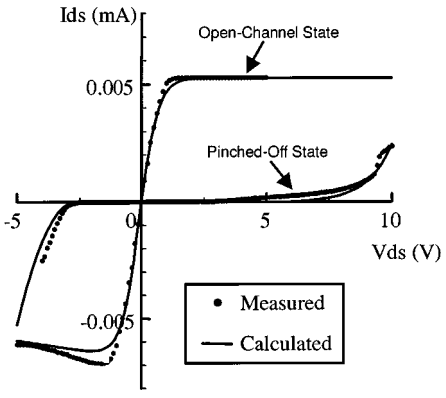

Fig. 13. Current source characteristics for unit FET.

TABLE II
PARAMETER VALUES FOR TWO-TERMINAL NONLINEAR UNIT FET

ϕ_B	0.31 V
α	1.4 V^{-1}
β	9.55E-4 A/V^2
γ	1.3 V^{-1}
κ_f	0.001 V^{-1}
κ_r	1 V^{-1}
V_T	-2.35 V
R_{ISO}	5000000 Ω
Is_G	0.000007 A
Is_D	0.01 A
V_B	5.7 V
Vgs_O	0 V
Vgs_P	-5.0 V

The large-signal transmission characteristics of the TWSW was simulated using the harmonic-balance method on HP MDS. For both the ON and OFF states, the simulated results are in good agreement with the measured data, as shown in Fig. 10. In the large-signal simulation, the inductance of the bonding wires from the input/output ports to the test fixture has been considered. The insertion loss increased by about 2.4 dB due to introducing the bonding wires.

The simulated results teach us that the degradation of the isolation with respect to the input power level is caused by the current saturation of the open-channel-state FET at the knee voltage. As the input power level increases, the current saturation arises at the signal-input port area and the current saturation area is extended to the signal-output port. The isolation degrades with the increase of the input power level since the characteristic impedance Z of the TWSW decreases. In this model, the source–drain capacitance of the FET assumes to be a constant, but the practical capacitance varies with respect to the input voltage level. For a more accurate model, the voltage-dependent capacitance model should be considered.

VI. Conclusion

The MMIC TWSW has been developed for millimeter-wave applications. The presented lossy transmission-line model for the TWSW successfully explained the measured results. The developed 400-μm TWSW showed insertion losses of less than 2.55 dB and isolations of over 22.2 dB with monotonic increase over 40 dB from dc to 110 GHz. At 40 GHz, the power-handling capability of the TWSW was measured with no degradation of the insertion loss up to a 26.5-dBm input level. The large-signal model of the TWSW using a two-terminal nonlinear FET model successfully expressed the measured isolation degradation with respect to the input power level. The measured switching speed of the TWSW was less than 600 ps for a rise time and less than 400 ps for a fall time. The developed TWSW can successfully provide the broadest band MMIC switch with high power-handling capability and high switching speed for millimeter-wave communication and radar applications.

Acknowledgment

The authors would like to thank M. Ogawa, H. Hirayama, S. Agu, K. Uetake, and H. Fujisawa for helpful encouragement, K. Ohata, M. Kuzuhara, M. Funabashi, T. Saryo, and K. Maruhashi for technical discussions, and Y. Hori for metallizing processing.

References

[1] M. J. Schindler and A. Morris, "DC–40-GHz and 20–40-GHz MMIC SPDT Switches," *IEEE Trans. Microwave Theory Tech.*, vol. MTT-35, pp. 1486–1493, Dec. 1987.

[2] G. L. Lan, D. L. Dunn, J. C. Chen, C. K. Pao, and D. C. Wang, "A high-performance V-band monolithic FET transmit–receive switch," in *IEEE Microwave Millimeter-Wave Monolithic Circuits Symp. Dig.*, 1988, pp. 99–101.

[3] H. Takasu, F. Sasaki, H. Kawasaki, H. Tokuda, and S. Kamihashi, "W-band SPST transistor switches," in *IEEE Microwave Guided Wave Lett.*, vol. 6, Sept. 1996, pp. 315–316.

[4] M. Madihian, L. Desclos, K. Maruhashi, K. Onda, and M. Kuzuhara, "A high-speed resonance-type FET transceiver switch for millimeter-wave band wireless networks," in *Proc. 26th European Microwave Conf.*, Sept. 1996, pp. 941–944.

[5] H. Mizutani, M. Funabashi, M. Kuzuharad, and Y. Takayama, "Compact DC–60-GHz HJFET MMIC switches using ohmic electrode-sharing technology," *IEEE Trans. Microwave Theory Tech.*, vol. 46, pp. 1597–1603, Nov. 1998.

[6] Y. Ayasli, J. L. Vorhaus, R. A. Pucel, and L. D. Reynolds, "Monolithic GaAs distributed FET switch circuits," presented at the IEEE GaAs Integrated Circuit Symp., San Diego, CA, Oct. 27, 1981.

[7] N. Samoto, Y. Makino, K. Onda, E. Mizuki, and T. Itoh, "A novel electron-beam exposure technique for 0.1 μm T-shaped gate fabrication," *J. Vac. Sci. Technol.*, vol. B8, pp. 1335–1338, 1990.

[8] Y. Hori, K. Onda, M. Funabashi, H. Mizutani, K. Maruhashi, A. Fujihara, K. Hosoya, T. Inoue, and M. Kuzuhara, "Manufacturable and reliable millimeter-wave HJFET MMIC technology using novel 0.15 μm MoTiPtAu gates," in *IEEE MTT-S Int. Microwave Symp. Dig.*, 1995, pp. 431–434.

[9] H. Mizutani and Y. Takayama, "A DC-60 GHz GaAs MMIC switch using novel distributed FET," in *IEEE MTT-S Int. Microwave Symp. Dig.*, Denver, CO, June 1997, pp. 439–442.

Hiroshi Mizutani (M'97) received the B.S. and M.S. degrees from Kyoto University, Kyoto, Japan, in 1986 and 1988, respectively.

In 1988, he joined the NEC Corporation, Kawasaki, Japan, where he has been engaged in the development of GaAs process technology, development of GaAs power MESFET's, and research and development of millimeter-wave GaAs MMIC's. He is currently an Assistant Manager in the C&C LSI Development Division. His current interest includes millimeter-wave MMIC's, especially novel switch circuits for millimeter-wave applications.

Mr. Mizutani is a member of the Institute of Electronics, Information and Communication Engineers (IEICE), Japan.

Yoichiro Takayama (M'72) received the B.S., M.S., and Dr.Eng. degrees from Osaka University, Osaka, Japan, in 1965, 1967, and 1973, respectively.

In 1967, he joined the Central Research Laboratories, NEC Corporation, Kawasaki, Japan, and was engaged in the research and development of Gunn and IMPATT diode application technology from 1969 to 1974, and GaAs FET circuit technology from 1974 to 1980. From 1980 to 1986, he was responsible for the research and development of microwave GaAs FET's, heterojunction bipolar transistors (HBT's), MMIC's, and compound semiconductor digital circuit technologies. In 1986, he joined the Semiconductor Group, NEC Corporation, Kawasaki, Japan, where he has been engaged in the development of microwave and optical semiconductor devices. He is currently the Chief Engineer of the Semiconductor Group.

Dr. Takayama received the 1983 Microwave Prize presented by the IEEE Microwave Theory and Techniques Society (IEEE MTT-S).